WORLD CONFERENCE ON TIMBER ENGINEERING 2025
BRISBANE, AUSTRALIA

Advancing Timber for the Future Built Environment

EVALUATIONS FROM MULTIPLE PERSPECTIVES ON TIMBER-CONCRETE COMPOSITE SLABS FOCUSING ON ADHESION WATERPROOF COATINGS

Yukiko Nakatsu[1], Shuhei Uesugi[2], Katsuhide Murakami[3], Yoshisato Esaka[4]

ABSTRACT: This study provides a comprehensive examination of Timber-Concrete Composite (TCC) floors, which are a combination of wooden materials used for formwork and concrete slabs. TCC floors have been gaining popularity due to their structural advantage of enabling thinner slab thickness and the recent trend towards the use of wood in buildings. In practical construction scenarios, wooden formwork laid on beams is temporarily left outdoors, making it desirable to apply waterproof paint on the upper surface of the wooden formwork (the boundary between the wooden formwork and the concrete slab). The waterproof coating also serves to prevent the moisture in the concrete from penetrating the wooden formwork. Through the course of the research, it was found that waterproof coatings based on vinylester contribute to the integration of the wooden formwork and the concrete slab. Floors in buildings are required to have not only structural performance but also fire resistance, living performance, and sound insulation performance. Therefore, a multifaceted evaluation of TCC floors, considering the adhesion of the waterproof coating, was attempted. Specifically, element tests and four-point bending tests were conducted with the parameters of wooden members, concrete slab thickness, and joint conditions. In addition, long-term creep tests for half a year, living performance tests by heel impact and walking vibration measurement, and tests for heavy and lightweight floor impact sound insulation performance were carried out.

KEYWORDS: wood material, reinforced concrete, painting, loading test, creep test

1 – INTRODUCTION

For floors, which are the most widely used component in buildings, we will develop a composite floor that satisfies the performance requirements for use by consumers, while at the same time using a low carbon emission wood material. In Japan, detailed consideration of the fact that no interference in use will occur can be omitted for floor members by satisfying a minimum of 1/30 of the span. Therefore, the span of the timber-concrete composite floor to be developed in this study should be about 3 m, and the thickness of the RC section should be at least 100 mm and at least 1/30 of the span. For occupant performance (walking vibration, etc.), which is considered by the designer outside the law, the floor should satisfy the requirements by taking into account the composite effect of the wood and RC sections. Specifically, the floor should be designed to have integral bending rigidity for long-term loads and small deformations, and when considering vertical movement during a major earthquake, the system should be designed to ensure safety through the composite effect of out-of-plane deformation performance and out-of-plane bearing capacity through screws, etc.

[1] Yukiko Nakatsu, Engineering Dept, Structural Design Division, NIKKEN SEKKEI Ltd. , Tokyo, Japan, nakatsu.yukiko@nikken.jp

[2] Shuhei Uesugi, Engineering Dept, Structural Design Division, NIKKEN SEKKEI Ltd. , Tokyo, Japan, uesugi.shuhei@nikken.jp

[3] Katsuhide Murakami, Director, Engineering Dept, Structural Design Division, NIKKEN SEKKEI Ltd. , Dr.Eng. Tokyo, Japan, murakamik@nikken.jp

[4] Yoshisato Esaka, Director, Engineering Dept, Structural Design Division, NIKKEN SEKKEI Ltd. , Dr.Agr. Tokyo, Japan, esakay@nikken.jp

https://doi.org/10.52202/080513-0354

Figure 1 shows an overview of a timber-concrete composite floor. TCC floors are fire resistant only in the concrete section. To reduce the effect of moisture on the wood during concrete placement and to ensure the integrity of the wood and concrete during micro-deformation, a film-forming vinylester waterproof coating (product name: Xyladecol Conzolan) was applied to the contact surface between the wood and concrete to improve the adhesion performance of the interface. The test was conducted for a 3 m span, and two types were tested: a CLT type (RC section: 100-120 mm + 3-layer 4-ply CLT section: 120 mm thick) and a Joist type (RC section: 100mm + Joist section: 30mm thick + 120 mm thick), which efficiently reduces the amount of wood used. Both of these TCC floors are assumed to have an equivalent RC floor thickness of 140 mm.

2– ELEMENTAL SHEAR TESTS

We conducted elemental shear tests to verify the performance of painted and shear resisting screws applied to the wood-concrete interface. Based on the results of preliminary tests, the screws were of the form of a V shape (diagonal cross casting), in which the screws are driven into each other at a 45 degree angle to form a V shape, which has relatively high bonding performance with the concrete. The test pattern was designed to show the adhesion performance of the waterproofing paint and the shear performance of the diagonally crossed screws (see Table 1). Here, specimens No.1 and 2 have Teflon sheets between CLT and concrete, which is a measure to cut the adhesion between CLT and concrete.

The materials used in the elemental shear tests are listed in Table 2, and the geometry of the elemental shear specimens is shown in Figure 2. Table 3 shows the maximum loads and Figure 3 shows the load-deformation curves for each test. It was confirmed that the adhesion performance of the vinylester waterproofing coating applied to the boundary surface with the concrete during the initial deformation was higher than the integrity effect

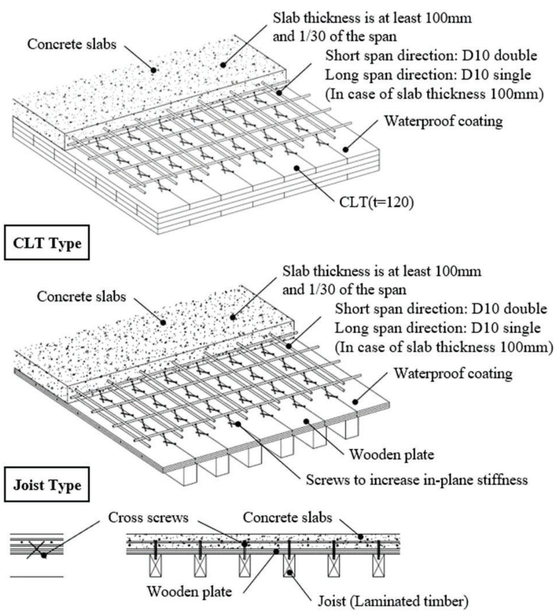

Figure 1. Structural Concept Diagram

Table 1. Element Shear Test Specimens

No.	Between CLT and RC	Shear Mechanism				CLT	number of specimens
		Screw	Embedded length	Angle	number		
①	Waterploof paint＋Teflon sheets	MPAS-180	100	45	2	Strong Axis	3
②	Waterploof paint＋Teflon sheets	MPAS-180	100	45	2	Weak Axis	3
③	Waterploof paint	MPAS-180	100	45	2	Strong Axis	3
④	Waterploof paint	MPAS-180	100	45	2	Weak Axis	3
⑤	None	MPAS-180	100	45	2	Strong Axis	3
⑥	None	MPAS-180	100	45	2	Weak Axis	3
⑦	Waterploof paint	None				Strong Axis	3
⑧	None	None				Strong Axis	3

Table 2. List of Materials (Element Shear Test)

Component Name	Specification	Remarks
Concrete	Ordinary concrete	Fc21 (Design σ_c=21 N/mm^2)
CLT	CLT composed of Cryptomeria japonica D.D.	Mx60 3-layer-4-ply, Japanese cedar
Waterproof paint	Xyladecol Conzolan	-
Screw	MPAS-180	outer diameter 8.4mm, length 180mm
Teflon sheets	UHMW-PE No.4430	width 100mm, thickness 0.16mm

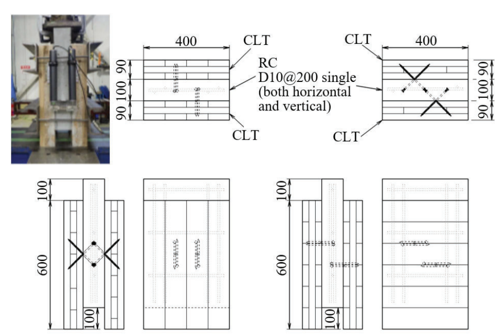

Figure 2. Specimens(Element Shear Test) and Photograph

Table 3. Maximum Load (Element Shear Specimens)

No.	Specimens	Maximum Load (kN)	No.	Specimens	Maximum Load (kN)
①	1	31.17	⑤	1	41.59
	2	31.14		2	36.31
	3	29.58		3	39.68
	average	30.63		average	39.19
②	1	26.70	⑥	1	25.94
	2	21.96		2	26.80
	3	24.40		3	25.97
	average	24.35		average	26.24
③	1	51.65	⑦	1	42.10
	2	38.73		2	27.22
	3	57.98		3	34.26
	average	49.45		average	34.53
④	1	26.18	⑧	1	26.66
	2	28.92		2	18.78
	3	29.95		3	16.08
	average	28.35		average	20.51

https://doi.org/10.52202/080513-0354

of the screws, both in terms of bearing capacity and stiffness.

3 – FOUR-POINT BENDING TESTS

3.1 Speciments and Loading Equipment

Four-point bending tests of near full-scale specimens were conducted to determine the ultimate bending capacity of the composite floor. Table 4 lists the specimens. The specimens were subjected to five conditions: positive bending specimens with a wood member (CLT or lumber) on the bottom and concrete on the top, negative bending specimens with the reverse arrangement, and RC slabs only, some of which were subjected to creep tests. The number of specimens was three for specimens 1-8 and 14-18, and only one for specimens 9-13. The negative bending specimens were conducted to determine the performance of the slab edges because when wood is used as formwork during construction, tensile edge stresses occur in the wood at the center of the slab, but top-end tensile bending moments occur at the slab edges, and compressive edge stresses occur in the wood.

Figure 4 shows the overview of specimen 5 as a representative specimen; the CLT was 0.4 m wide and 2.7m long, with 3-layer, 4-ply Japanese cedar Mx60 (F_b=11.51 N/mm^2) CLT boards (@30 x 4 = 120 mm) that were glued together with resorcinol-based adhesives in width-breaking glue, and the joists were Japanese cedar laminated wood equivalent to E60 (F_b=13.8 N/mm^2). Concrete thickness was 100-120mm, and steel bars were D10 (σ_y=295 N/mm^2). Since the wood surfaces were exposed to wind and rain during construction and moisture during concrete placement could affect the wood surfaces, vinylester weatherproof paint was applied to the interface between the wood and concrete (except for specimens 9-13). The vinylester-based paint has strong adhesive properties and is expected to reduce the in-plane shear displacement of the boundary surface between the wood and concrete. However, in consideration of safety against vertical movement, etc., during a major earthquake, screws (MP All Screw) 180 mm long and 8.4 mm in outermost diameter were driven in at an angle to increase the in-plane shear rigidity between the wood and concrete.

As shown in Figure 4, the boundary condition was a pin-supported bearing at the end of the specimen that allowed rotation around the Y-axis. The bending stiffness of the composite floor was calculated using the theory of superimposed beams [1]. When calculating the bending stiffness, the in-plane shear stiffness between the wood and

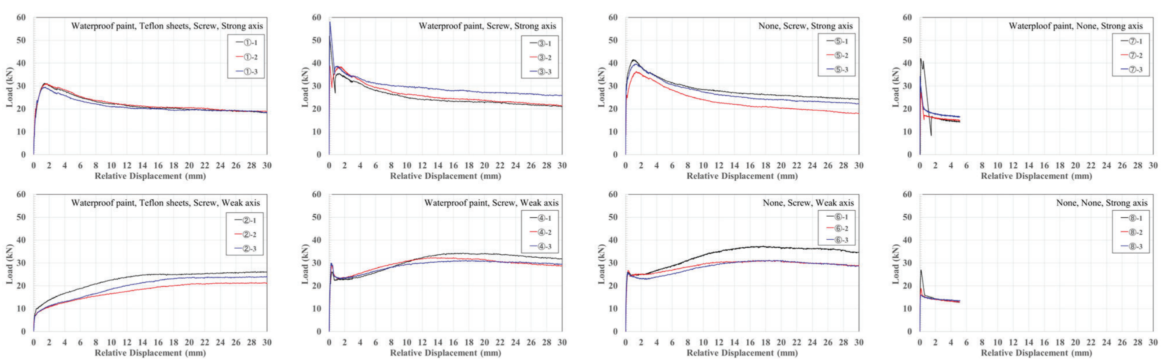

Figure 3. Load-Displacement Relationship (Element Shear Specimens)

Table 4. List of Specimens (Four-Point Bending Tests)

No.	Wood Type	RC thickness (mm)	Over-all Length (mm)	Distance between fulcrums (mm)	Upper edge	Upper center	Lower edge	Lower center	Orthgonal Reinforcing Bars	Concrete Type	Loading Method	Pitch of screw (mm)	E_eI_e / E_cI_c	Number of specimens	Remarks
1	CLT	120	2600	2280	@200	@200	@200	@200	double	Plain Fc21	forward	200	2.70	3	
2			3600	3270	@200	@200	@200	@100※			backward			3	
3	Joist	100	2400	2100	@200	@200	@200	@200	single	Plain Fc21	forward	200	4.18	3	
4			3200	2880	@200	@200	@200	@100※			backward	200		3	
5			2400	2100	@200	@200	@200	@200			forward	400		3	
6												400 staggered		3	
7	CLT	100	2400	2100	@200	@200	@200	@200	single	Plain Fc21	forward	400	3.49	3	
8	Joist	100	2400	2100	@200	@200	@200	@200	single	Lightweight 1 Lc21	forward	400	5.01	3	
9	—	100	2400	2100	@200	@200	@200	@200	single	Plain Fc21	forward	—	1.00	1	only concrete slab
10		100	3200	2880							backward			1	only concrete slab
11		140	2400	2100							forward			1	only concrete slab
12		100	2400	2100	@200 single	@200 single	@200 single	@200 single	single		forward			1	only concrete slab
13	CLT	120	2400	2100	@200	@200	@200	@200	single	Plain Fc21	forward	400	2.70	1	no warterploof paint
14	CLT	100	2400	2100	@200	@200	@200	@200	single	Plain Fc21	forward	400	3.49	3	after half-year creep test (Load: 5800kg/m^2)
15	Joist									Plain Fc21			4.18	3	after half-year creep test (Load: 5800kg/m^2)
16										Lightweight 1 Lc21			5.01	3	after half-year creep test (Load: 5800kg/m^2)
17														3	after half-year creep test (Load: 2900kg/m^2)
18										Plain Fc21			4.18	3	after one-year creep test (Load: 5800kg/m^2)

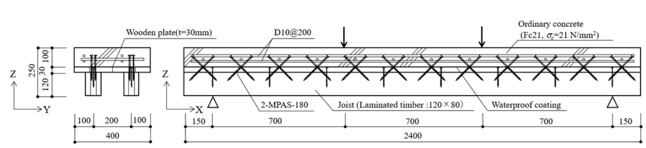

Figure 4. Specimen (Example：Specimen-5)

concrete was assumed to be infinite, and the composite beam was assumed to be fully composite with plane retention. The ratio of the bending stiffness E_eI_e of the composite floor to the bending stiffness E_cI_c of the RC slab alone for each specimen is shown in Table 4.

3.2 Test Results of Four-point Loading Test

Figure 5-9 show the relationship between vertical load (sum of two points) and vertical displacement (displacement at the point of application) for specimens 1-18. The elastic stiffness K_e of the composite slab calculated using the bending stiffness E_eI_e and the vertical load P_1 when the center of the RC slab reaches the long -term allowable bending moment are also shown. Figure 10 shows a comparison of the concrete sections with different type of wood, and Figure 12 shows a comparison of TCC floors with and without coating. In both specimens, the initial stiffness K_1 (the range before delamination occurs) tended to be slightly greater than K_e, but this may be due to the fact that the actual bearing capacity of the wood and concrete is greater than the design value. Due to delamination of the waterproof paint at the concrete interface, the load was reduced about bearing capacity in both specimens. The order of occurrence of delamination tended to be at the beam ends for the first and second load drops and at the center of the beam for the third load drop. After the concrete and wood delaminated along the entire length, cross screws contributed to prevent in-plane displacement. No misalignment was observed at the interface between the wood and concrete under vertical loads of P_1 or less. Comparing specimen 3 with specimens 5 and 6, no significant differences in stiffness and bearing capacity were observed before the first delamination, but the number of screws affected the stiffness after the delamination occurred, and the degree of load reduction varied depending on the number of diagonal screws. Compared to the specimens with only RC slabs, the initial stiffness and vertical bearing capacity of all composite slab specimens are higher due to the composite effect, regardless of the loading direction. Furthermore, even after a creep test with a loading period of six months to one year, the properties of the load-deformation curves are the same.

From Figure 10, it can be seen that the lightweight concrete timber composite floor has a slightly lower load level than the normal concrete timber composite floor, indicating that the displacement at the concrete interface occurs at a slightly lower load level than the normal concrete timber composite floor. Figure 11 shows that in negative bending, the concrete side becomes the tensile side, so the deformation region where the initial stiffness is demonstrated is not as wide as in positive bending, and after the concrete cracks, both stiffness and vertical bearing capacity are not as high because they are affected by the tensile capacity of the steel bars. Furthermore, Figure 12 shows that the initial stiffness is maintained up to larger deformations when the interface is coated compared to the uncoated case, suggesting that the vinylester coating contributes to the synthesis effect.

3.3 Building Analytical Model

The versatile structural analysis software Midas iGen (ver. 900 R1x) was used to reproduce specimen 1. Figure 13 shows the outline of the analysis model. The stiffness of the RC section was evaluated as a concrete cross-section, and the stiiffness of the CLT and concrete was determined from the design base strength. The in-plane stiffness K of the diagonal screws was calculated from ETA [2] (without considering concrete strength or thickness).

$$\boldsymbol{K = 85 l_{ef}} \qquad (1)$$

where l_{ef} is effective length of screw (mm).

The wood material (CLT) was isotropic material, and the shear modulus automatically calculated from Young's modulus was set to match the design value of the shear modulus by using the stiffness increase factor. A tension-only spring equivalent to the shear stiffness given in (1) was placed between the wood and concrete in the form of a brace. The boundary condition was pin support at the support points, and the external force was set to 100 kN at the sum of the two points. To check the effect of shear stiffness between concrete and wood members on the composite floor, Model 1 was created with shear stiffness equivalent to actual screw placement, and Model 2 was created with infinite shear stiffness at the interface. Figure 14 shows the analysis results. The bending moment diagram shows that the RC slab mainly bears the external forces. The vertical displacements at the loading point of the beams in Model 1 and Model 2 are 10.3mm ($K=P/\delta=9.71$ kN/mm) and 5.8 mm ($K=17.4$ kN/mm),

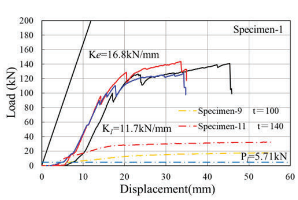

Figure 5. Forward Specimen-1

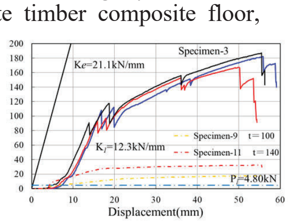

Figure 6. Forward Specimen-3

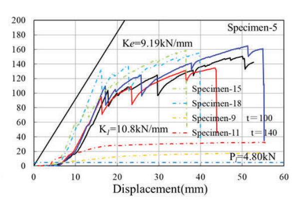

Figure 7. Forward Specimen-5

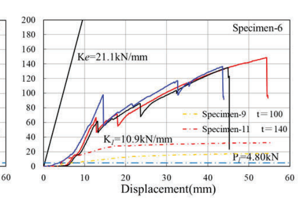

Figure 8. Forward Specimen-6

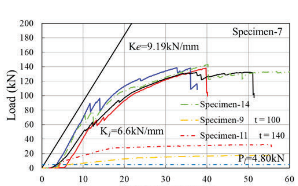

Figure 9. Forward Specimen-7

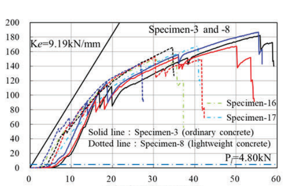

Figure 10. Comparison of Concrete

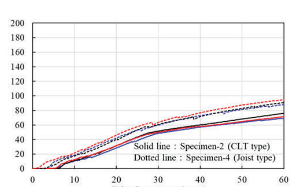

Figure 11. Backward

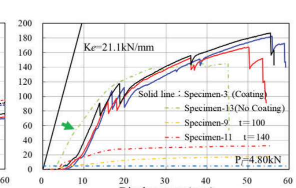

Figure 12. Comparison of Coating

https://doi.org/10.52202/080513-0354

respectively, and it is analytically confirmed that the higher the shear elastic stiffness, the smaller the vertical displacement. On the other hand, the average initial stiffness of specimen 1 is K_1=11.7 kN/mm, so the shear stiffness of the actual interface is considered to be intermediate between the shear stiffness equivalent to a screw arrangement and the shear stiffness of the interface being infinite.

4 – BENDING CREEP TEST

To determine the long-term flexural performance of timber-concrete composite floors, we conducted flexural creep tests indoors and evaluated the creep performance using the Power law. Twelve flexural creep specimens were tested, one per condition. The TCC floors were divided into two major types, CLT type and Joist type, and the concrete thicknesses of the CLT type and the Joist type were different, 120 mm and 100 mm, respectively. The specimen specifications and loading conditions are shown in Table 5, and the specimen diagram is shown in Figure 15. Deflection measurements were made with a displacement transducer installed on the underside of the center of the specimen span. We started to take measurements at the time when the concrete was placed, and after a curing period of 27 days, the specimens were loaded according to the loading conditions. For the negative bending specimens, the specimens were inverted before loading. The test site was not a constant-temperature, constant-humidity room, and although not directly exposed to rainwater, it was affected by fluctuations in outside temperature and humidity, so the temperature and humidity near the specimens were measured continuously to determine if there was any effect on deformation. The test period was 180 days (259200 minutes).

The relationship between creep deformation and the passage of time during the test period is shown in Figure 16. All specimens deformed rapidly from the time the concrete was placed to the time it cured, but after 27 days, when the concrete had generally cured, the deformation was not so severe even when load was applied. For the negative bending specimens, both CLT and Joist types tended to deform in the opposite direction of gravity for about 50 days after inversion. This may be due to the fact that the deformation was oriented by the deflection of the wood material due to the weight of the uncured concrete, and the shrinkage of the concrete continued after the inversion, causing the deformation to progress into an

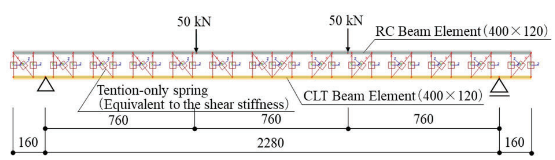

Figure 13. Analytical Model

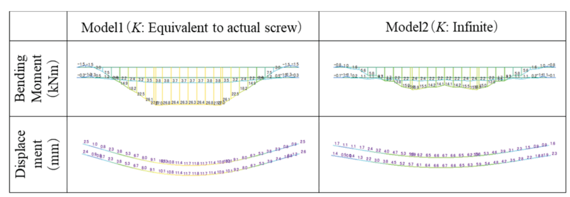

Figure 14. Analysis Results

Table 5. List of Specimens (Bending Creep Tests)

Specimen ID	Type	RC thickness (mm)	Loading Method	Load (N/m^2)	Length (mm)	Bar arrangement	Pitch of screw (mm)	Concrete Type	Coating	Loading Period
C-1	CLT	120	Forward	5800	2000	Double	200	Ordinary, Fc21	Xyladecol Conzolan	Harf year
C-2	CLT	120	Forward	2900	2000	Double	200	Ordinary, Fc21	Xyladecol Conzolan	Harf year
C-3	CLT	120	Backward	2900	2900	Double	200	Ordinary, Fc21	Xyladecol Conzolan	Harf year
C-4	CLT	120	Forward	5800	2000	Double	200	Ordinary, Fc21	No Coating＋wetted	Harf year
C-5	Joist	100	Forward	5800	1700	Single	200	Ordinary, Fc21	Xyladecol Conzolan	1 year
C-6	Joist	100	Forward	2900	1700	Single	200	Ordinary, Fc21	Xyladecol Conzolan	Harf year
C-7	Joist	100	Backward	2900	2500	Single	200	Ordinary, Fc21	Xyladecol Conzolan	1 year
C-8	CLT	100	Forward	5800	2000	Single	400	Ordinary, Fc21	Xyladecol Conzolan	Harf year
C-9	Joist	100	Forward	5800	2000	Single	400	Ordinary, Fc21	Xyladecol Conzolan	Harf year
C-10	Joist	100	Forward	5800	1700	Single	400	Lightweight, Lc21	Xyladecol Conzolan	Harf year
C-11	Joist	100	Forward	2900	1700	Single	400	Lightweight, Lc21	Xyladecol Conzolan	Harf year
C-12	Joist	100	Backward	2900	2500	Single	400	Lightweight, Lc21	Xyladecol Conzolan	Harf year

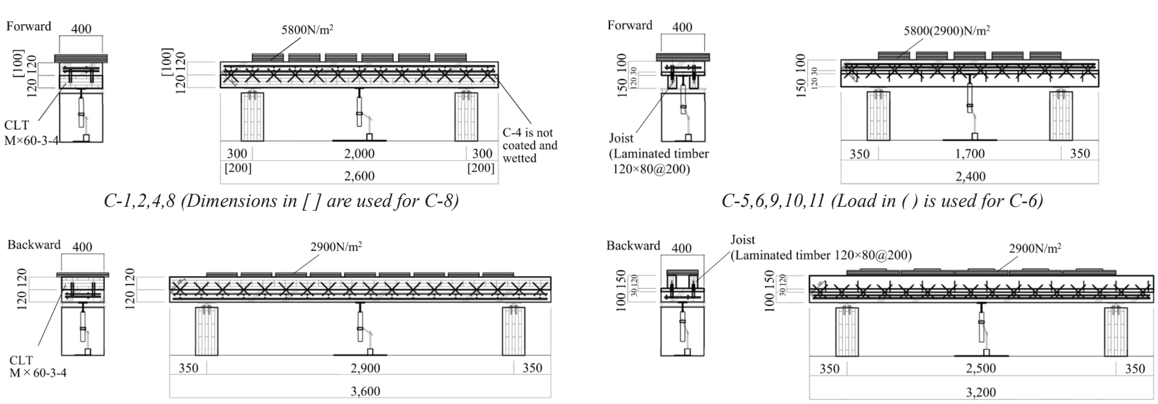

C-1,2,4,8 (Dimensions in [ ] are used for C-8)

C-5,6,9,10,11 (Load in ( ) is used for C-6)

C-3

C-7,12

Figure 15. Diagram of Bending Creep Tests

arched shape. The presence or absence of waterproof coating had no obvious effect on the deformation, and it is considered that the deformation of the specimens before and after loading was influenced by the individual differences in the bending performance of the wood panels acting as the formwork.

The measured results were applied to the Power law to predict the coefficient of increase in deformation for a loading duration of 50 years. The prediction was made by calculating the initial deflection as the displacement after loading, with the starting point before loading after the concrete had hardened. The CLT type positive bending specimens and the Joist type positive bending specimens could be calculated, but the negative bending specimens of both types could not be applied to the Power law formula because the displacement was measured to be in the direction of the ceiling and the amount of deflection decreased with time. Especially in the case of negative bending, the drying shrinkage of the concrete on the lower (tensile) side is considered to have a significant effect. Figure 17 shows the predicted creep after 50 years obtained using the Power law, and Table 6 lists the predicted results for each specimen. The rate of deformation increase tended to be greater for the CLT type than for the Joist type, suggesting that the rate of deformation increase for the CLT type may exceed that of concrete by a factor of 16.

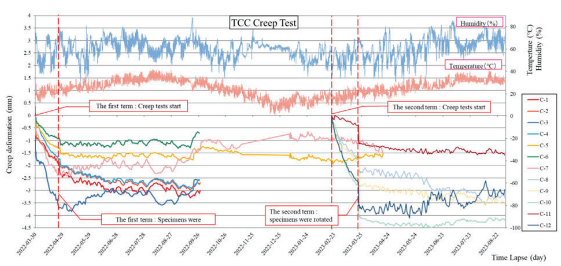

Figure 16. Creep deformation - Time

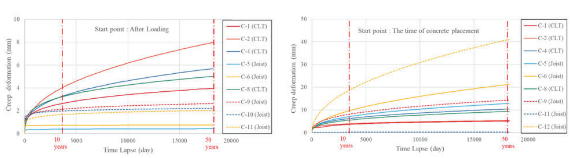

(a) Start point : After Loading

(b) Start point : The time of Concrete placement

Figure 17. Predicted Creep Deformation after 50 years by Power Law

Table 6. Prediction of Each Specimen

Specimen ID	C-1	C-2	C-3	C-4	C-5	C-6	C-7	C-8	C-9	C-10	C-11	C-12
Type	CLT	CLT	CLT	CLT	Joist	Joist	Joist	CLT	Joist	Joist	Joist	Joist
Term1 (N/m^2)	5800	2900	2900	5800	5800	2900	2900	5800	5800	5800	2900	2900
Term2(Forward: F, Backward: B)	F	F	B	F	F	F	B	F	F	F	F	B
(a) Prediction when the stat point is after concrete hardening												
Initial deflection δ_0	0.40	0.16	0.34	0.27	0.24	0.17	0.20	0.20	0.67	0.65	0.59	0.67
Defrection after 50 years δ_{50}	3.97	7.98	-	5.70	0.43	0.76	-	5.02	2.64	2.22	2.04	-
δ_{50}/δ_0	9.93	49.89	-	21.10	1.81	4.47	-	25.08	3.94	3.42	3.46	-
(b) Prediction when the start point is at the time of concrete placement												
Initial deflection δ_0	0.76	0.79	1.45	0.40	0.28	0.10	0.44	0.36	0.39	0.11	0.18	0.32
Defrection after 50 years δ_{50}	4.44	4.72	10.82	11.06	14.64	28.28	38.33	9.50	17.02	310.4	0.03	66.60
δ_{50}/δ_0	5.85	5.98	7.47	27.65	52.30	282.8	87.10	26.39	43.65	2822	0.16	208.1

5 – MEASUREMENTS OF VERTICAL VIBRATION CHARACTERISTICS OF TCC FLOORS

The specimens C-2, C-3, and C-6 used in the creep test were subjected to vibration by heel excitation about 7 months after concrete was placed to measure the vertical acceleration of the floor surface and analyze the natural frequency and damping constant of the floor. Photograph 1 shows the scene of the measurement. The acceleration was measured at the center of the specimen (No.2) and at two points 300mm away from No.2 in the longitudinal direction (No.1 and No.3), for a total of three points. Vibration was applied between No.1 and No.2 and between No.2 and No.3 as shown in the photographs. The excitation was performed with a pin-supported bearing in place at the fulcrum position of the specimen during the creep test.

5.1 Natural Frequency

Figure 18 shows the Fourier spectrum of each specimen obtained from the acceleration waveform measured at No.2. Since there were no significant differences in the measurement results at measurement points No.1-3 for any of the specimens, the results from No.2 will be used in the analysis. The frequencies at which the Fourier amplitudes are dominant are different for each specimen. Specimens C-2 and C-3 have two distinct peaks, whereas specimen C-6 has three distinct peaks. Here, the natural frequency of each specimen is calculated by the gravity equation using the stiffness of the concrete/wood interface as a single unit. Table 7 shows the frequencies obtained from the measurements and analysis. The vibration frequency *f* was calculated by the following equation (2) and (3).

$$f = c/\sqrt{\delta} \qquad (2)\ [3]$$

$$\delta = 5wl^4/(384EI) \qquad (3)$$

where *c* is constant(=5.62), δ is deflection of specimen, *w* is dead weight of specimen and *EI* is bending stiffness of specimen. The *w*, *l*, and *EI* used in the calculations are shown in the respective graphs in Figure 18. Regarding the first-order natural frequencies obtained by each calculation method, it can be seen that for specimens C-2 and C-3, the frequencies obtained by the heel excitation and gravity

Photo 1. Measuring scenary (C-2)

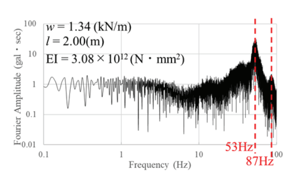

(a) C-2 (CLT)

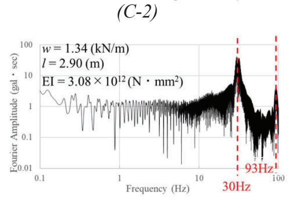

(b) C-3 (CLT,turned over)

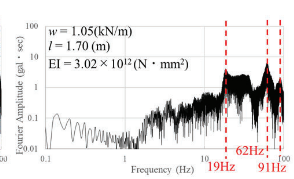

(c) C-6 (Joist)

Figure 18. Fourier Spectra

https://doi.org/10.52202/080513-0354

equations generally correspond to each other. In specimen C-6, three predominant frequencies are observed, but the primary natural frequency is considered to be 62 Hz as read from the measured Fourier spectrum. On the other hand, the gravity equation calculated a frequency of 92 Hz, which is close to the measured second-order natural frequency. The results for specimen C-6 will be the subject of further study.

5.2 Damping Ratio

Figure 19 shows the free vibration waveforms measured at the No.2 position of each specimen during excitation. In addition, the damping constants and damping curves are shown when the amplitude ratio is calculated as the average of 10 and 20 cycles. The damping constants *h* were identified as *h*=0.032 and 0.040 for specimen C-2, *h*=0.034 and 0.030 for specimen C-3, and *h*=0.031 and 0.027 for specimen C-6. However, the damping curve for specimen C-6 corresponds to the peak value of the free vibration waveform, while specimens C-2 and C-3 have curves that deviate from the peak value. This may be due to the fact that in the free vibration waveform of specimen C-6, the amplitude gradually decreases and then approaches zero, whereas in specimens C-2 and C-3, the large amplitude at the beginning of the free vibration waveform decays once, but the amplitude increases again before it fully decays. The amplification of vibration can be attributed to the following reasons. Specimen C-6 is a type of slab with joists attached to the concrete, and shows approximate RC slab characteristics. On the other hand, specimens C-2 and C-3 are completely composed of two layers of concrete and CLT, and it is considered that the vibration given to the top surface of the specimens not only transmitted from the concrete to the CLT or from the CLT to the concrete, but also partially reflected vibration was transmitted to the accelerometer placed on the top surface of the specimens. The initial waveforms of specimens C-2 and C-6 showed similar decreasing trends, but specimen C-3 showed a slower decrease than the other two and a sudden decrease at around 0.2 sec.

5.3 Walking Vibration Measurement

Vertical vibrations caused by heel excitation and walking vibration are measured on a specimen of timber-concrete composite floor to understand the vibration characteristics of the slab and to evaluate the habitability of the slab.

Figure 20 shows overviews of the slab specimen and the locations where heel excitation and walking vibration were measured. The floor slab specimen is assumed to be half the size of a room floor in a real building. The Fourier spectrum obtained by heel excitation is shown in Figure 21, and the natural frequencies of the CLT and Joist types are almost the same, except that the Fourier amplitude is larger at 10 Hz for the CLT type. Figure 22 shows the free vibration waveforms measured for each specimen. Also shown are the damping constants and damping curves when the amplitude ratio is calculated as the average of 10 and 20 cycles. Similar to the beam element specimens shown in Section 5.2, the CLT type specimens also exhibit a phenomenon in which the amplitude increases again in the middle of the free vibration in the floor slab specimens.

Next, in order to understand the habitability of TCC floors, walking vibration measurements were conducted by actually walking on the floor slab specimens. The excitation force for walking was assumed to be that of a single adult walking with a typical body weight, with four case speeds of 1.8 Hz, 2.0 Hz, 2.2 Hz, and 2.2 Hz for the CLT type and 1.9 Hz, 2.1 Hz, 2.3 Hz, and 2.5 Hz for the Joist type. Figure 23 shows the results of 1/3-octave band analysis calculated from the measured acceleration waveform. In Japan, performance evaluation curves [5]

Table 7. Natural Frequency by each method

Specimen ID	Type	Natural frequency (Hz)	
		Actual measurement	Analysis
		Vibration by heel	Fomula
C-2	CLT	53, [87]	59
C-3	CLT (turned over)	30, [93]	28
C-6	Joist	62, [19], [91]	92

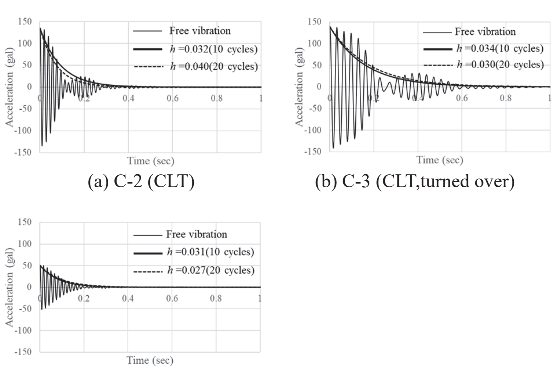

(a) C-2 (CLT)

(b) C-3 (CLT,turned over)

(c) C-6 (Joist)

Figure 19. Free Vibrations and Damping Curves

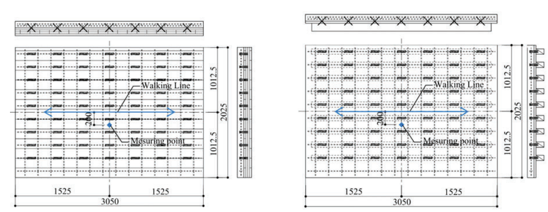

(a) CLT

(b) Joist

Figure 20. Specimen for Walking Vibration Mesurement

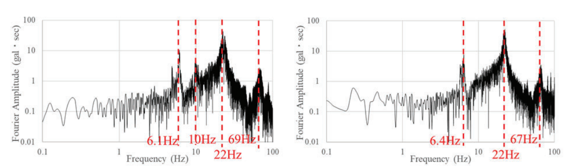

(a) CLT

(b) Joist

Figure 21. Fourie Spectra (floor specimen)

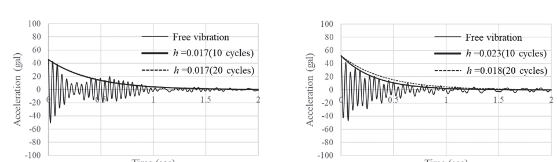

(a) CLT

(b) Joist

Figure 22. Free Vibration and Damping Curve (floor specimen)

defined on the basis of vibration perception probability are used to check the occupant performance of floors. The evaluation curves for vertical vibration are defined as V-10.V-30, V-50, V-70, and V-90. This index expresses what percentage of people at the point being evaluated will feel each level of vibration when it occurs. For example, V-10 indicates that the vibration level is felt by 10% of the people at the point. The maximum acceleration values from the 1/3-octave band analysis are plotted for each 1/3-octave band center frequency and superimposed on the performance evaluation curve to determine the floor occupancy performance. For the CLT type, the maximum value of acceleration increases to about V-90 around 6Hz, 10Hz, and 20Hz, while for the Joist type, it is about V-90 around 6Hz and 20Hz. It can be seen that the acceleration increases near the natural frequency obtained by heel excitation. As mentioned above, V-90 is the level at which 90% of people would feel vibration and be quite concerned about it, which means that the performance is not suitable for an office room. On the other hand, the support condition of the end of the specimen in this study is that it is only placed on a stand, and the fact that it will be fixed to a beam when applied to an actual building was not taken into consideration, which may have resulted in a larger-than-expected result.

Therefore, we create analytical models of the slab specimens and compare it with the measured results to see how much the acceleration is reduced when the edge anchorage is taken into account. The analytical model is modeled using the general-purpose analytical model Midas iGen (ver. 900 R1x) as in Chapter 3. However, since the shear stiffness between the RC and CLT due to the waterproof coating is considered to be sufficiently large based on previous verifications, the RC and CLT are modeled as a single plate element in the model to simulate walking vibration, assuming that they are a single unit. The CLT and concrete properties are calculated using values obtained from the design basis strength. The modeling of plate elements is as follows; First, the Young's modulus E_{in} and shear modulus G_{in} in the in-plane direction are determined by (4) and (5), respectively, considering the thickness of RC and CLT. In the tool, the shear modulus is automatically calculated based on Young's modulus and Poisson's ratio (G_{auto}), so it is adjusted by the increase/decrease factor α_1 obtained by (6) to equal the value obtained by (5).

$$E_{in} = \left(t_{rc} \times E_{rc} + t_{strong} \times E_{strong} + t_{weak} \times E_{weak}\right) / \left(t_{rc} + t_{strong} + t_{weak} \right) \quad (4)$$

$$G_{in} = \left(t_{rc} \times G_{rc} + t_{strong} \times G_{strong} + t_{weak} \times G_{weak}\right) / \left(t_{rc} + t_{strong} + t_{weak} \right) \quad (5)$$

$$\alpha_1 = G_{in}/G_{auto} \quad (6)$$

Next, Young's modulus E_{out} and shear modulus G_{out} in the out-of-plane direction are calculated based on the theory of superposed beams. However, since the plate elements are modeled using isotropic materials, the Young's modulus and shear modulus in the out-of-plane direction are adjusted by increasing/decreasing factors α_2 to α_5, taking into account the strong and weak axes of the CLT, so that the values calculated based on the layered beam theory are used for Young's modulus and shear stiffness, respectively [4]. Table 8 shows the various parameters of the analytical model. The excitation force is a load simulating a single adult walking (walking speed 1.8 Hz to 2.5 Hz, in 0.2 Hz increments), applied at the center node of the specimen, and a time history analysis is performed.

The results of the eigenvalue analysis are shown in Figure 24. the first-order natural frequency is slightly lower than the measured value, but this may be due to the fact that the Young's modulus of the specimen wood is larger than the design value. However, the natural frequencies around 6Hz and 10Hz, which were confirmed in the measured results, were not confirmed in the analysis. The results of the walking vibration analysis are shown in Figure 25. (a)

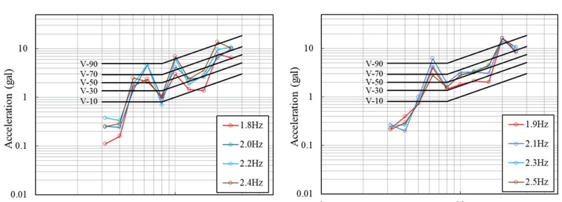

(a) CLT Type (b) Joist Type

Figure 23. Octarve Band Analysis (walking alone)

Table 8. Specifications of Analysis Model (CLT Type)

Content	Character	Value	Unit
Young's modulus of concrete	E_{rc}	21682	N/mm^2
Young's modulus of CLT strong axis	E_{strong}	6000	N/mm^2
Young's modulus of CLT weak axis	E_{weak}	0	N/mm^2
Elastic shear modulus of concrete	G_{rc}	8339	N/mm^2
Elastic shear modulus of CLT	G_{strong}, G_{weak}	500	N/mm^2
Thickness of concrete	t_{rc}	100	mm
Thickness of CLT strong axis	t_{strong}	60	mm
Thickness of CLT weak axis	t_{weak}	60	mm
G_{in} / G_{auto}	α_1	0.919	(-)
Correction factor for out-of-plane bending stiffness (strong axis)	α_2	0.618	(-)
Correction factor for out-of-plane bending stiffness (weak axis)	α_3	0.554	(-)
Correction factor for out-of-plane shear stiffness (strong axis)	α_4	0.0143	(-)
Correction factor for out-of-plane shear stiffness (weak axis)	α_5	0.0117	(-)

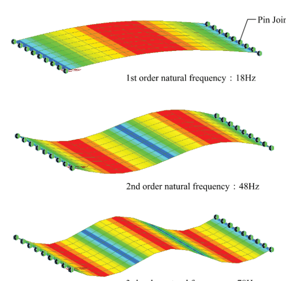

Figure 24. Eigenvalue Analysis (CLT Type)

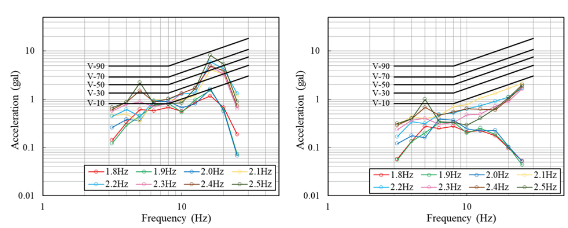

(a) Pin-joint (b) Rigid-joint

Figure 25. Octarve Band Analysis (CLT Type, walking alone)

https://doi.org/10.52202/080513-0354

shows the results for the case where the support conditions at the ends are pin-jointed on the short sides and free on the long sides to simulate the actual measurement conditions, and (b) shows the results for the case where the four sides are rigidly jointed, assuming the actual construction. The result of (a) shows that the maximum acceleration value is close to V-90 at a frequency of 16 Hz, although the vibration frequency at which the acceleration reaches its maximum value is different from the actual measurement, which is considered to roughly simulate the actual measurement results. In the case of four-round fixation, the maximum value is less than V-30. In reality, the occupancy performance is considered to be in the range of V-30 to V-70, taking into account the fact that the building is not fully fixed. This performance would not be a problem if TCC floors were installed in an office building.

6 – LABORATORY MEASUREMENTS OF FLOOR IMPACT SOUND INSULATION PERFORMANCE

Because securing floor impact sound insulation performance is likely to be an issue for timber floors, timber-concrete composite floors, etc., the performance of heavy-weight and light-weight floor impact sound insulation in CLT-type and Joist-type timber-concrete composite floors was tested. The test site was an acoustic building in accordance with JIS A 1440-1 and -2 (Figure 26), with the two types of specimens shown in Figure 27. Here, JIS is an abbreviation for Japanese Industrial Standards. Two specimens of the almost same size as those in Section 5.3 were placed side by side, and the space between and around the two specimens were sealed with clay. The excitation points were set in two patterns: large and small.

The test specimens were struck with a tapping machine and a bang machine in accordance with JIS A 1418 (2000), and the sound pressure levels at five points in the lower chamber were measured with a sound level meter to obtain energy averaged values.

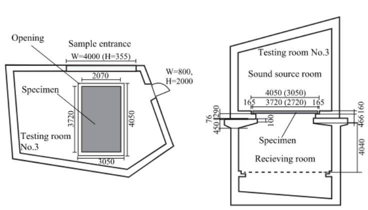

Figure 26. Laboratory Plan and Elevation (unit : mm)

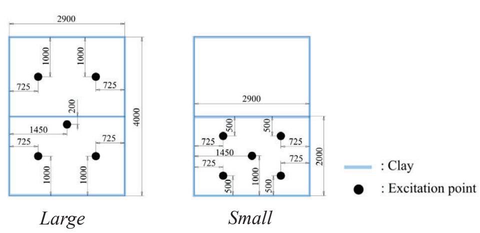

Figure 27. Specimens for Acoustical Tests (unit：mm)

The results are shown in Figure 28. For reference, the evaluation was performed using the grading curve shown in JIS A1419-2 (2000). The sound insulation performance for heavy floor impact noise is Lr-55 for both the CLT and Joist types. Here, Lr is an index to evaluate the performance against floor impact noise in Japan, and Lr-55 corresponds to excellent sound insulation performance when the building use is a school or an office. Since the lightweight floor impact sound insulation performance is greatly affected by the finish, the test specimens, which are bare concrete, exceeded the evaluation curve by a large margin as expected. When this timber-concrete composite floor is used in a living room, it is necessary to reduce lightweight floor impact noise by means of floor finish and installation of a subfloor ceiling. The difference between the large and small vibration patterns was not significant enough to affect the grade evaluation for both heavy and lightweight floors.

7 – CONCLUSION

The performance of TCC floors using vinylester-based waterproof coatings was evaluated from multiple perspectives, and the following findings were obtained.

Four-point bending tests showed that vinylester-based waterproof coatings enhance the composite effect at the interface between timber material and concrete. Due to the effect of this coating contributing to the integration of the RC slab and wood members, the K_e calculated under the assumption of a fully composite beam tended to be greater than the initial stiffness before delamination occurred. The number of screws had a limited effect on the initial stiffness, but did affect the stiffness after delamination.

The flexural creep test of the timber-concrete composite concrete was more significant than the effect of the wood in the creep evaluation.

The measured natural frequencies of the vertical direction of the timber-concrete composite floors generally corresponded to the analysis. In terms of damping characteristics, the free vibration waveform of the Joist type smoothly approaches zero due to damping, but the CLT type exhibits a buzzing phenomenon in which the amplitude is amplified again during the damping process. This is considered to be an effect of not only transmission but also reflection of vibrations between the concrete and CLT.

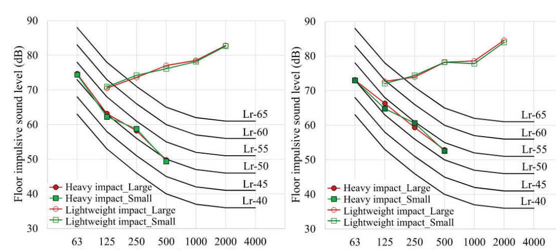

(a) CLT Type (b) Joist Type

Figure 28. Heavy and Lightweight Floor Impacts Sound Insulation Performance

The measured occupant performance of the floor slab specimens in walking vibration measurements generally corresponded to the analysis. Although the measured occupant performance was low, the analysis showed high occupant performance when the support conditions were changed to those assumed for actual construction, suggesting that the timber-concrete composite floor has acceptable occupant performance.

The sound insulation performance of the timber-concrete composite floor with a concrete thickness of 100 mm was Lr-55 for both the CLT and Joist types. This corresponds to excellent sound insulation performance when the building use is a school or an office.

8 – REFERENCES

[1] Architectural Institute of Japan. “Fundamental Theory of Timber Engineering”, 2010.

[2] European Technical Assessment ETA-19/0244

[3] Kiyoshi Muto, “Dynamic analysis of structures”, Maruzen Publishing Co., Ltd., 4th ed., 1966.

[4] FPInnovations, Canadian CLT Handbook, 2019 EDITION. https://web.fpinnovations.ca/wp-content/uploads/clt-handbook-complete-version-en-low.pdf (accessed March 12, 2025).

[5] Architectural Institute of Japan. “Guidelines for the evaluation of habitability to building vibration” , 2004.

https://doi.org/10.52202/080513-0354